

Simulated Pion Photoproduction Experiments

by

Ethan Howe

Submitted to the Department of Physics in partial fulfillment of the Requirements for
the Degree of

Bachelor of Science

at the

Massachusetts Institute of Technology

May, 2005 [June 2005]

© 2005 Ethan Howe
All Rights Reserved

The author hereby grants to MIT permission to reproduce and to distribute publicly
paper and electronic copies of this thesis document in the whole or in part.

Signature of Author _____

May 20, 2005
Department of Physics
(Date of signature)

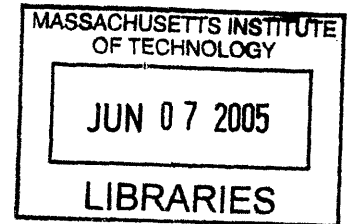
Certified by _____

[Signature]
Professor Aron Bernstein
Thesis Supervisor, Department of Physics

Accepted by _____

Professor David E. Pritchard
Senior Thesis Coordinator, Department of Physics

ARCHIVES



Simulated Pion Photoproduction Experiments

Ethan Howe
MIT Department of Physics
(Dated: May 20, 2005)

I present the details of my simulation for the proposed polarized target, polarized photon, pion photoproduction experiment at the new HI γ S facility. This experiment will make important measurements of the multipoles for pion production in the near threshold region which will shed light on chiral symmetry breaking. I detail the parameters of the NMS detector to be used for the experiment including its acceptance and resolution. I reproduce the cross section that we are hoping to measure. I present the results of fitting the cross section coefficients by two different methods and compare their accuracy. I conclude by discussing further improvements that will be made to my simulation by future students investigating this experiment.

Contents

1. Introduction	1
1.1. Polarized Cross Section	2
2. Simulation Details	4
2.1. The NMS Detector	6
3. Fit Results	11
4. Conclusions and Future Work	16
References	18
5. Acknowledgements	18
A. Simulation Script Names and Functions	25

1. INTRODUCTION

In this paper, I will be assessing the capabilities of the Neutral Meson Spectrometer (NMS) detector in a planned experiment at the High Intensity Gamma Source (HI γ S) at Duke University. I will review the relevant theory and set out the importance of this experiment. I will describe the proposed apparatus and how I have modeled it in my simulation. I will explain the data we wish to draw from the experiment and present results as to how well I believe this setup will perform.

This experiment will be the first to measure many of the double-polarization observables for pion photoproduction in the near threshold region. The production of pions depends on the strong force, which is described by quantum chromodynamics (QCD). For light mesons, an effective field theory called Chiral Perturbation Theory (ChPT) has been developed, which calculates a perturbative approximation to QCD. The mass of the quarks results in the breaking of chiral symmetry. The neutral pion (π_0) is the lightest meson and thus is closest to the chiral limit. The production of π_0 will shed light on spontaneous chiral symmetry breaking in QCD, a fundamental part of the structure of matter. Isospin is particularly interesting in chiral dynamics. Isospin is a fundamentally conserved quantity that explains many disallowed processes in particle physics. The violation of isospin due to the differences in up and down quark masses in the pion photoproduction system was predicted twenty years ago by Weinberg.[2] The measurement of the

polarized cross section will allow determination of the amount of isospin breaking in the ΠN system. There are several competing theoretical models that predict the observables for this system in the near threshold region. In addition to ChPT one loop, there are MAID [6] and DMT [7] model calculations. These theoretical and model calculations will be stringently tested by the future HI γ S data.

1.1. Polarized Cross Section

The differential cross section for pion photoproduction has the form shown in figure 1 where each R is an observable of the reaction, the h_e in front of the last term is the helicity of the photon beam, p_π^* and k_γ^* are the center of mass momenta of the pion and photon, respectively.[4] [5]

$$d\sigma/d\Omega^* = p_\pi^*/k_\gamma^* \{ R_T + P_n \mathbf{R}_T^n + \Pi_T [(R_{TT} + P_n \mathbf{R}_{TT}^n) \cos 2\Phi - (P_l \mathbf{R}_{TT}^l + P_t \mathbf{R}_{TT}^t) \sin 2\Phi] + h_e \Pi_C (P_l R_{TT'}^l + P_t R_{TT'}^t) \} \quad (1)$$

Π_T and Π_C are the amounts of photon linear and circular polarization, respectively, on a scale from zero to one. The P terms are determined by the amount and direction of target polarization being used. We have chosen to define these terms relative to the lab frame so that we get the following values: If the target is polarized normal to the plane of the floor $P_n = P_T \cos(\phi_\pi)$, $P_t = P_T \sin(\phi_\pi)$, and $P_l = 0$ where P_T is the amount of target polarization again on a zero to one scale. If the target is polarized perpendicular to the beam, in the plane of the floor, then $P_n = -P_T \sin(\phi_\pi)$, $P_t = P_T \cos(\phi_\pi)$, and $P_l = 0$. If the target is polarized along the beam then $P_n = P_t = 0$, and $P_l = P_T$. ϕ_π is the pion azimuthal angle in the lab frame and Φ is the angle between the photon polarization and the plane of the photoproduction reaction. For photons polarized in the plane of the floor $\Phi = \phi_\pi$ and for photons polarized perpendicular to the floor $\Phi = 2\pi - \phi_\pi$. R_T is the unpolarized observable and R_{TT} and R_T^n are the single polarization observables. R_T has been measured in many experiments in the threshold region but R_{TT} has only been measured only once so far for π_0 . [1] It is important to note that this measurement of R_{TT} disagreed with the predictions of DMT. In the HI γ S experiment, we would like to verify or dismiss this discrepancy. The five double polarization observables will also be accessible although R_{TT}^n , R_{TT}^l , and R_{TT}^t are all relatively small and will be hard to measure accurately. These observables can be defined in terms of the complex S and P wave multipoles of the interaction E_{0+} , E_{1+} , M_{1+} , and M_{1-} . Examples of these expansions are shown in the following equations where θ is the center of mass pion polar angle:

$$R_T = |E_{0+}|^2 + \frac{1}{2} \left(|2M_{1+} + M_{1-}|^2 + |3E_{1+} - M_{1+} + M_{1-}|^2 \right) \quad (2)$$

$$+ 2 \cos(\theta) \Re \{ E_{0+}^* (3E_{1+} - M_{1+} + M_{1-}) \}$$

$$+ \cos^2(\theta) (|3E_{1+} - M_{1+} + M_{1-}|^2$$

$$- \frac{1}{2} (|2M_{1+} + M_{1-}|^2 + |3E_{1+} - M_{1+} + M_{1-}|^2))$$

$$R_T^n = 3 \sin(\theta) \Im \{ E_{0+}^* (E_{1+} - M_{1+}) \} \quad (3)$$

$$- \cos(\theta) (E_{1+}^* (4M_{1+} - M_{1-}) + M_{1+}^* M_{1-})$$

$$R_{TT} = 3 \sin^2(\theta) \left(\frac{3}{2} |E_{1+}|^2 - \frac{1}{2} |M_{1+}|^2 - \Re \{ E_{1+}^* (M_{1+} - M_{1-}) + M_{1+}^* M_{1-} \} \right) \quad (4)$$

$$R_{TT}^n = \sin(\theta) \Im \{ E_{0+}^* (3E_{1+} + M_{1+} + 2M_{1-}) + 3 \cos(\theta) M_{1-} (3E_{1+}^* + M_{1+}^*) \} \quad (5)$$

The terms of these expansions can be grouped together into coefficients that multiply each function of θ . These coefficients are shown in equations 6-9 and their definitions can be deduced by comparison to the previous definitions.

$$R_T = a_T + b_T \cos(\theta) + c_T \cos^2(\theta) \quad (6)$$

$$R_T^n = \sin(\theta) (a_T^n + b_T^n \cos(\theta)) \quad (7)$$

$$R_{TT} = a_{TT} \sin^2(\theta) \quad (8)$$

$$R_{TT}^n = \sin(\theta) (a_{TT}^n + b_{TT}^n \cos(\theta)) \quad (9)$$

These multipoles and coefficients are the values that I will be fitting in the results section of the paper. Further, if we split up the terms of equation 1 according to the two polarizations, we can see which parts of the cross section we can isolate by flipping the polarizations. From this perspective there are three pieces: observables unchanged by polarization reversal, observables that change sign by target polarization reversal, and observables that change sign by both target and photon polarization reversal. These three groupings are shown in equation 10 where h_e is again the photon helicity and we have separated the target sign into the h_T helicity term.

$$h_T = \text{sign}(P_T) = \pm 1 \quad (10)$$

$$h_e = \pm 1$$

$$(d\sigma/d\Omega^*)_{h_T, h_e} = p_\pi^*/k_\gamma^* \{ R_T + \Pi_T R_{TT} \cos 2\Phi + h_T (P_n \mathbf{R}_T^n + \Pi_T [P_n \mathbf{R}_{TT}^n \cos 2\Phi$$

$$- (P_l \mathbf{R}_{TT}^l + P_t \mathbf{R}_{TT}^t) \sin 2\Phi] \} + h_T h_e \Pi_c (P_l R_{TT'}^l + P_t R_{TT'}^t)$$

We can use these degrees of freedom in the apparatus to eliminate different pieces of the cross section by subtracting data with different helicities. Equations 11-14 gives the four possible separations.

$$(d\sigma/d\Omega^*)_{1,1} - (d\sigma/d\Omega^*)_{1,-1} = p_\pi^*/k_\gamma^*(\Pi_c (P_l R_{TT'}^l + P_t R_{TT'}^t)) \quad (11)$$

$$(d\sigma/d\Omega^*)_{1,1} + (d\sigma/d\Omega^*)_{1,-1} = p_\pi^*/k_\gamma^* \{ R_T + \Pi_T R_{TT} \cos 2\Phi + (P_n \mathbf{R}_T^n + \Pi_T [P_n \mathbf{R}_{TT}^n \cos 2\Phi - (P_l \mathbf{R}_{TT}^l + P_t \mathbf{R}_{TT}^t) \sin 2\Phi]) \} \quad (12)$$

$$(d\sigma/d\Omega^*)_{1,1} + (d\sigma/d\Omega^*)_{1,-1} + (d\sigma/d\Omega^*)_{-1,1} + (d\sigma/d\Omega^*)_{-1,-1} = p_\pi^*/k_\gamma^* (R_T + \Pi_T R_{TT} \cos 2\Phi) \quad (13)$$

$$(d\sigma/d\Omega^*)_{1,1} + (d\sigma/d\Omega^*)_{1,-1} - (d\sigma/d\Omega^*)_{-1,1} - (d\sigma/d\Omega^*)_{-1,-1} = p_\pi^*/k_\gamma^* (P_n \mathbf{R}_T^n + \Pi_T [P_n \mathbf{R}_{TT}^n \cos 2\Phi - (P_l \mathbf{R}_{TT}^l + P_t \mathbf{R}_{TT}^t) \sin 2\Phi]) \quad (14)$$

Here, we see that we have a number of degrees of freedom in the way we use the polarizations for the apparatus. We can keep the same polarizations over a whole run and examine the overall cross section. Alternatively, we can split the run time up into portions with different polarizations and then subtract the cross sections from each run and fit each of the above pieces separately. Now that I have described the motivation, goals, and theory behind this experiment, I will detail the apparatus proposed to make these measurements.

2. SIMULATION DETAILS

Before the actual experiment begins, we need some understanding of what we can expect from our apparatus. To get an idea of these expectations, I have created a simulation of data generation, detection, and analysis using the numerical package called ROOT. We pseudo-randomly generate certain unconstrained variables such as the phi angle of photon decay and other variables are also random but they fall within a certain probability distribution such as the cross section. Some details of the detector have been abstracted away into Gaussian or piecewise defined distributions. For instance, the errors produced from reconstructing photodetection across the crystals making up the detector have been simulated separately in GEANT and then imported as a table into my simulation.[8]

I split the simulation up into distinct parts. First, there are two pieces to every run, generation and analysis. I have separated these programs into two distinct scripts so that in theory when the experiment is performed the analysis script can be run on that data as easily as it can be run on the simulated data. These scripts can be found on the LNS network under the directory /export/lnan/data03/ethanhow/root. For more information on the name and use of each script, refer to appendix A. There are also two types of runs that are performed, acceptance and data. The acceptance run contains a much larger number of events to reduce statistical errors. The acceptance of the detector is found by knowing the input and output angles and dividing out the number of events that are detected in each angle bin. This process makes the acceptance independent of cross section and only dependent on the detector geometry. The data analysis uses the acceptance to reconstruct what the cross section should have been based on the percentage of counts we should have seen in each bin.

The simulation begins by calculating kinematic parameters of the interactions between the photon, proton, and pion. The photon energy is input as a constant and that energy and momentum is split between the recoil of the proton, the mass of the pion, and the kinetic energy of the pion. The proton is assumed to be stationary but a

future addition would be to add zero-mean thermal distribution to its momentum. These kinematics remain the same for all photoproduction events. The differences begin with the pion production polar and azimuthal angles, θ_π^* and ϕ_π^* , respectively. The stars superscripts denote that the angles are in the center of mass reference frame for the photoproduction reaction (referred to as the CM frame from now on). The pion angles depend on the cross section that was introduced in section 1.1. The differential cross section is in units of solid angle. I take this fact into account by multiplying the cross section by $\sin(\theta_\pi^*)$ and using bins of θ_π^* and ϕ_π^* in my analysis. Following its creation the pion will decay quickly into two photons. Since there are no outside interactions involved in this decay, the photons are produced back to back in the pion stationary frame. Thus one theta and phi define the photon decay process. These angles are uniformly random because there is no preferred direction of decay. Finally, I translate these angles that have been produced in different frames back to the laboratory where they are actually detected. The photon energies and momenta are Lorentz transformed from the pion frame to the CM frame using the energy-momentum four vector of the pion. The Lorentz transform is shown in equation 16 where β and γ define the magnitude of the transform. p (p') is the original (transformed) momentum, E (E') is the original (transformed) energy, and $i = x, y, z$ are the components of the vectors.

$$\begin{aligned} p'_i &= p_i + \gamma b_i \left(\frac{\gamma}{\gamma + 1} \vec{\beta} \cdot \vec{p} + E \right) \\ E' &= \gamma (E + \vec{\beta} \cdot \vec{p}) \end{aligned} \tag{15}$$

Then the CM frame is transformed to the lab frame by the photon energy. After these operations are complete, I have all the data that will be detected in the experiment, the angles and energies of both photons in the lab frame. In addition, I place the correct θ_π^* and ϕ_π^* in the data file so that I can check my calculations, and assess the accuracy of the detector. To determine the number of events created by the target, I use equation 17 where N_t is the areal density of the target, σ_{tot} is the total cross section, N_A is Avogadro's number, ρ_{target} is the density of the target, t is the run time, and I is the beam intensity.

$$\begin{aligned} N_t &= N_A * length_{target} * \rho_{target} \\ \sigma_{tot} &= 4\pi(a_T + c_T/3) \\ N_{events} &= t * I * N_t * \sigma_{tot} \end{aligned} \tag{16}$$

I used the following values for each of these variables based on our expectations of the final apparatus: $\rho_{target} = 0.0708$ for a liquid H_2 target, $I = 6 \times 10^6$ photons/second. For a run time of 100 hours, these numbers yield 1.43 million events. Next, we would like to know how many of these are actually detected by our detector.

2.1. The NMS Detector

The Neutral Meson Spectrometer (NMS) is the current proposed detector for this experiment. The NMS was built at Los Alamos Meson Physics Facility and it contains a number of systems that we will not be using at HI γ S. We will be stripping off vetoes, BGO crystals, and wire chambers that were present to improve the efficiency of the device. These devices were previously used to screen out charged particles and to improve the energy resolution. Our purposes require good position resolution to investigate asymmetries and the highest statistics we can achieve since the total cross section is small. For our setup, an array of cesium iodide crystals will remain. The detector is split into two arms placed on either side of the photon beam (see figures 1 and 2). Each arm of the detector is a 4×8 (x versus y) block of CsI crystals from total dimensions of 36×81 centimeters.

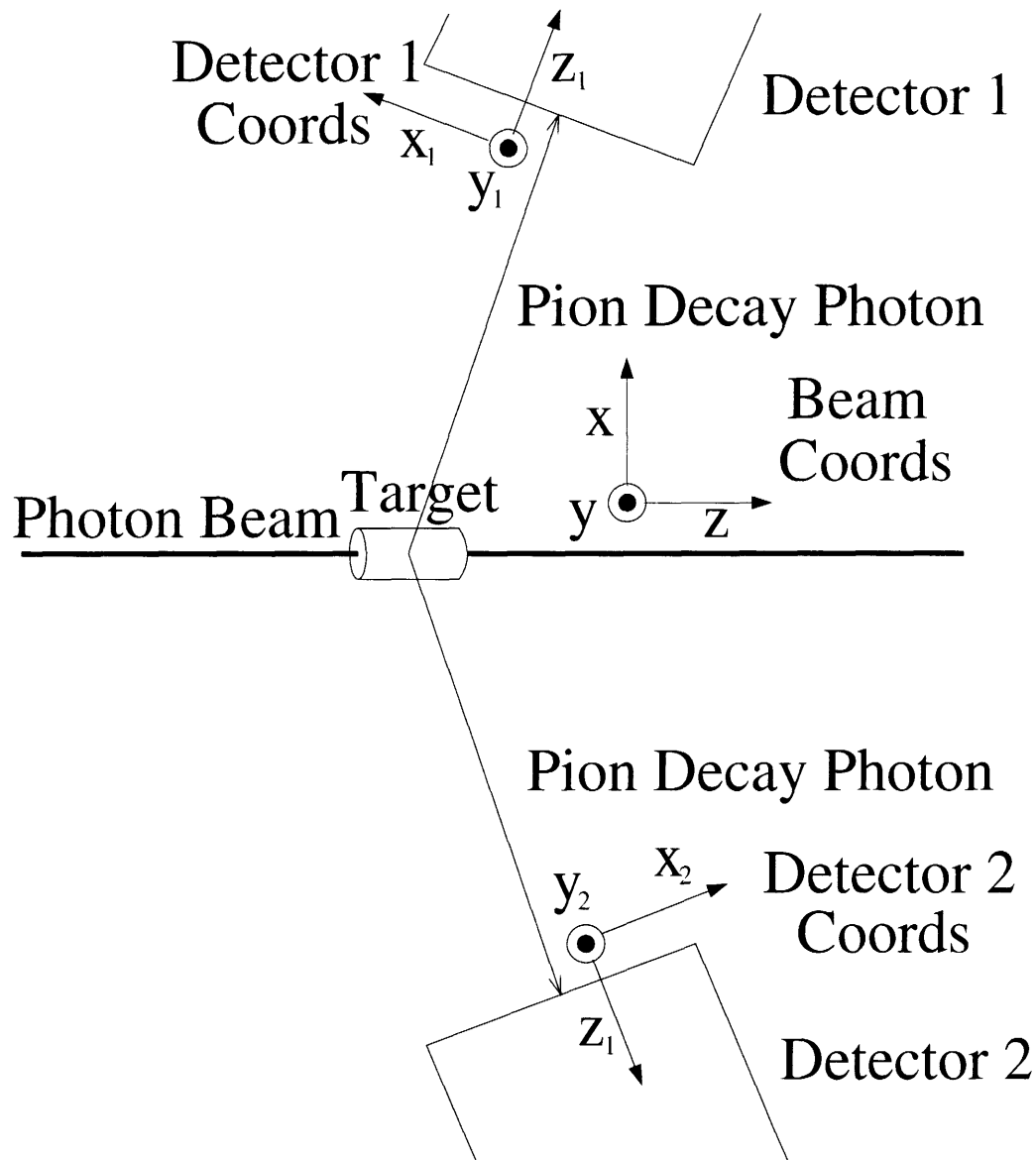


FIG. 1: The figure shows the proposed experimental apparatus. There are three coordinate systems, one for each detector and one for the lab. The laboratory floor is the x - z plane in all three coordinates.

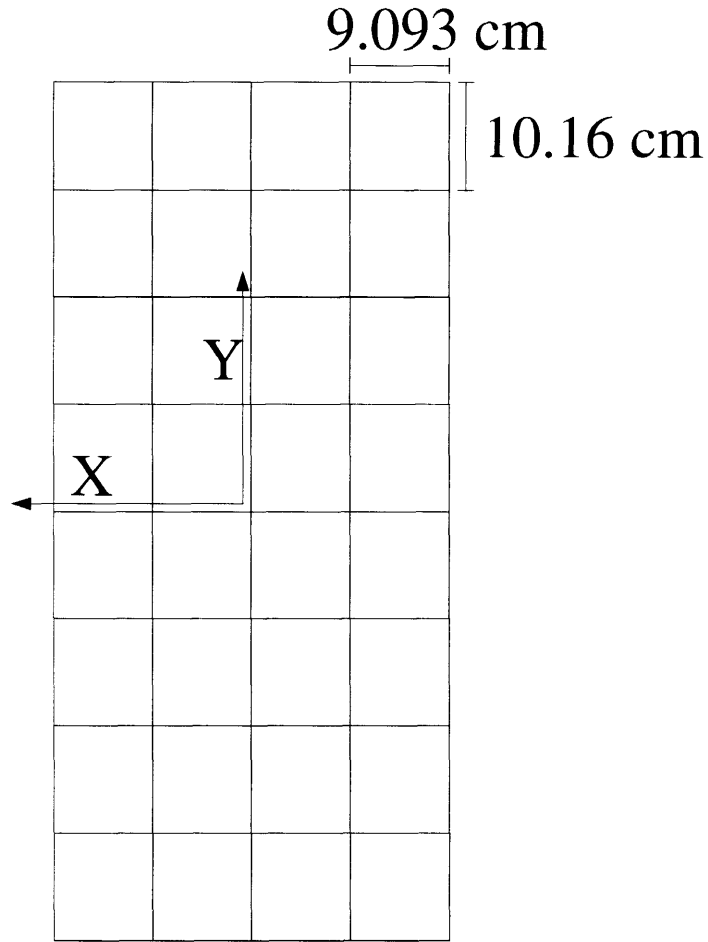


FIG. 2: The figure shows the face of the detector. There are 8 CsI crystals in the y direction and 4 crystals in the x directions. The crystals have slightly different dimensions in each direction. I assume that the face is completely flat in the current simulation.

The analysis script takes the raw data from the file and translates it to detected events. The script reads each event and calculates the position where the event strikes the detector from equation 18. R_d is the distance from the place the pion is produced to detector, θ_d is the angle between each detector arm and the beam, and θ_γ and ϕ_γ are the angles of the photon. Remember that θ_γ and ϕ_γ for each photon are what I record in the data file so that I could substitute a different detector by just changing equation 18 in the analysis code. The plus sign denotes the photon hitting detector 1 and the minus sign for detector 2. The difference corresponds to simply changing the sign of θ_d . The hit patterns on the detector faces calculated by these equations and generated by the polarized cross section are shown in figure 3.

$$x_d = \frac{-R_d(\pm \sin(\theta_d) \cos(\theta_\gamma) - \cos(\theta_d) \sin(\theta_\gamma) \cos(\phi_\gamma))}{\cos(\theta_d) \cos(\theta_\gamma) \pm \sin(\theta_d) \sin(\theta_\gamma) \cos(\phi_\gamma)} \quad (17)$$

$$y_d = \frac{R_d \sin(\theta_\gamma) \sin(\phi_\gamma)}{\pm \sin(\theta_d) \sin(\theta_\gamma) \cos(\phi_\gamma) + \cos(\theta_d) \cos(\theta_\gamma)}$$

If we had a perfect detector and a point target, then the data registered by the detector would be exactly determined by these equations. In the next step of analysis we add what errors we actually believe to see in the experiment. My simulation adds four types of error: x and y position, energy, and finite target. The x and y position error occurs

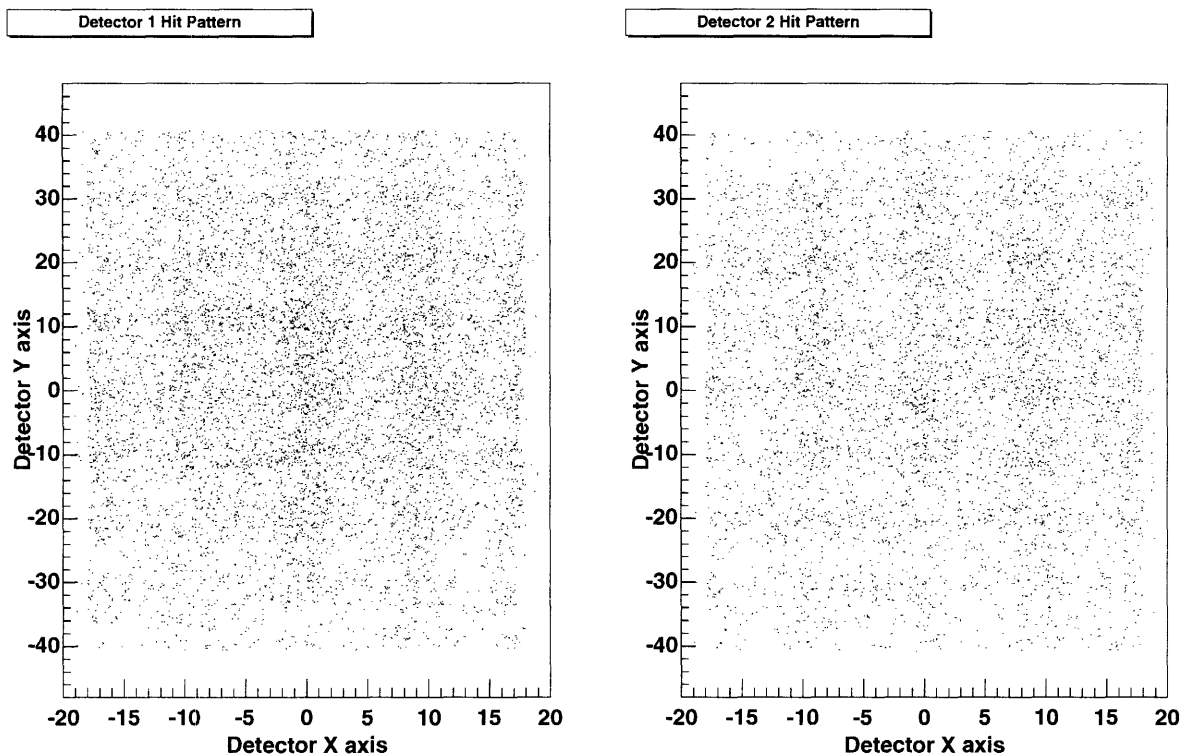


FIG. 3: Photon hit patterns for detector 1 and detector 2 on the left and right, respectively.

because of the difficulty in resolving the amount of energy deposited in the crystals surrounding the photon impact. The CsI crystals are not well designed for this task since their Molière radius is small compared to the dimensions of the crystal. Thus when a photon is absorbed in the middle of a crystal a very small amount of its energy spills into other crystals. The differences in energy distributed among crystals determines where the photon struck. Thus if the energy is contained only within one crystal then that photon must be assumed to be at the exact center of that crystal. Mohammed Ahmed has simulated these properties of the NMS detector and determined the average amount of error introduced depending on the location of the photon within each crystal.[8] Currently, I am not taking into account the fact that some photons will be placed directly in the center of a crystal but rather using the average errors at each position to generate a Gaussian displacement from the true location of the hit. This error is different in x and y since the crystals are longer in the y direction. You can see these errors in figure 4. The total energy detected for each photon is also subject to error. This error is proportional to the energy of the photon (see figure 5). Though you can see that the curve is concave so the error as a percentage of energy is decreasing because the photo-multipliers are more sensitive at larger energies. To factor these errors into the exact data, I sampled randomly from a Gaussian distribution with standard deviation equal values of the position and energy resolution functions. I then added the amount each returned to each variable independently. The last resolution comes from not knowing what position within the target that the pion is produced. I accounted for this unknown by choosing a uniformly random position along the length of the target for the pion to be produced and then changing the hit position of the photons with equation 19. These errors give the simulation its likeness to the real world and we are interested in their contributions to our analysis.

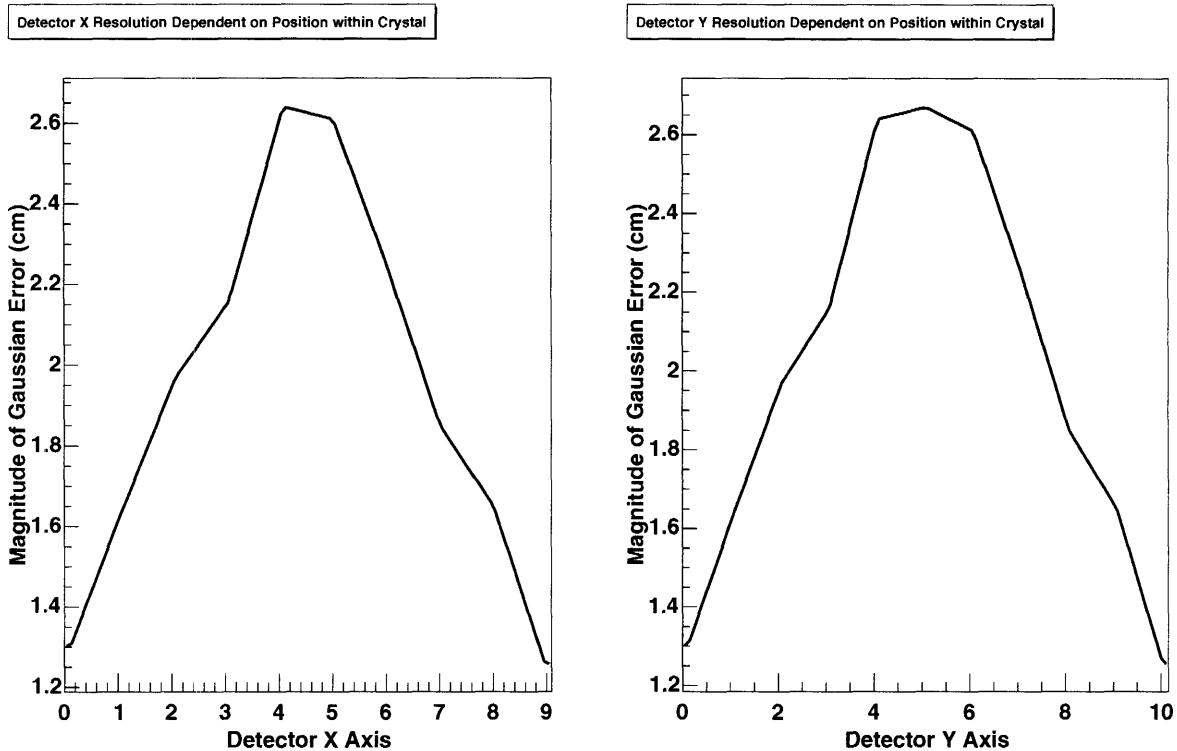


FIG. 4: The plots show the magnitude of Gaussian error added to the positions of detected photons based on their position with a particular crystal. The left and right plots represent the x and y axes, respectively.

$$z_{disp} = length_{target} \times (rand() - 0.5) \quad (18)$$

$$R'_d = R_d - z_{disp} \cos(\theta_d)$$

$$x'_d = x_d - z_{disp} \sin(\theta_d)$$

I define the detector acceptance as the percentage of pion production events that are detected. To have an event detected, both of the photons from the pion decay must be registered, one in either side of the detector. We have determined that the angle between the beam and each detector that detects the most events is approximately 81 degrees. To measure the acceptance of each bin in θ_π^* and ϕ_π^* , we create a data set that is an order of magnitude larger than our actual data set. The cross section of this data can be whatever the programmer wishes the only difference being in the bin errors of the acceptance. These errors should not matter much since the acceptance run has much higher statistics anyway. I ended up using a flat cross section so that I could get more counts in the low percentage bins. To find the acceptance, I run the analysis up to determining which photon pairs are detected. Then I take the pion angles from the data set and divide the number of detected pions over the number created pions in each angle bin. The acceptance is shown in figure 6. The acceptance depends on the energy of the photon beam and the geometry of the detector but nothing else since we are taking a ratio of detected events. To avoid the large errors associated with a small acceptance, I cut off the events analyzed at the ϕ_π^* bin where any percentage along the θ_π^* fell below 30%. Thus looking at the acceptance figure, only the green and red regions of the detected events were used.

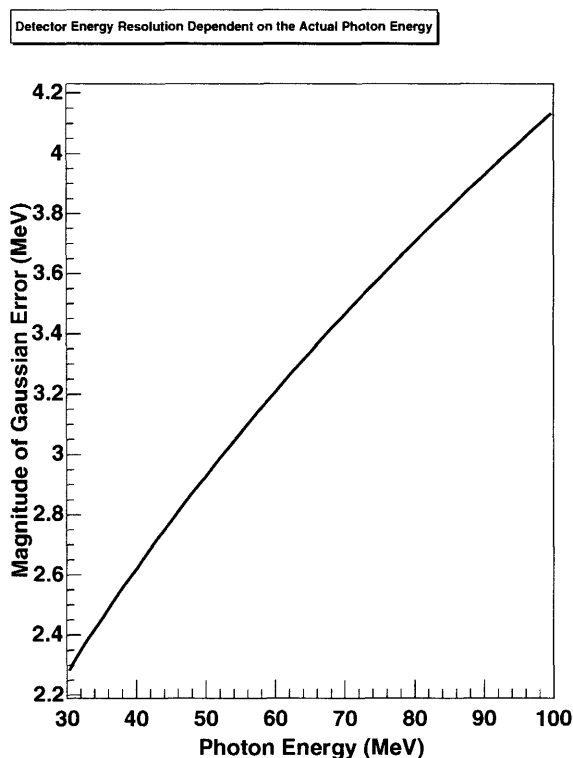


FIG. 5: The plot shows the absolute magnitude of the Gaussian error added to the photon energies

After we have gone through these steps, we can begin to examine the properties of our detector. First, we would like to make sure that the errors we have added are in fact on the order of magnitude we expect over all counts. Figure 7 shows the different types of error induced and their magnitudes for different cases averaged over a number of events. Next, we can examine how well we measure certain constants of the interaction. These include the sum of the photon energies and the missing mass defined by equation 19.

$$mm = \sqrt{2(e_1 \times e_2 - \vec{p}_1 \cdot \vec{p}_2)} \quad (19)$$

Both of these distribution have significant widths because of the inaccuracy of the energy measurement (see figure 8). Finally, we can calculate the pion CM angles from the positions of the detected events. This reconstruction uses equation 20 where $p_{\gamma x1}^*$ is the momentum of photon 1 in the CM frame. To get these photon momenta in the center of mass, I take the components of the photon momentum in the lab and use Lorentz transform in equation 16 on them with the known beam beta and gamma.

$$E^* = \sqrt{(p'_{\gamma x1} + p'_{\gamma x2})^2 + (p'_{\gamma y1} + p'_{\gamma y2})^2 + (p'_{\gamma z1} + p'_{\gamma z2})^2} \quad (20)$$

$$\theta_\pi^* = \arccos((p'_{\gamma z1} + p'_{\gamma z2})/E^*) \quad (21)$$

$$\phi_\pi^* = \arctan(p'_{\gamma y1} + p'_{\gamma y2} / p'_{\gamma x1} + p'_{\gamma x2}) \quad (22)$$

The distributions of the error in the reconstruction are shown in figure 9. Since we are examining the cross section of

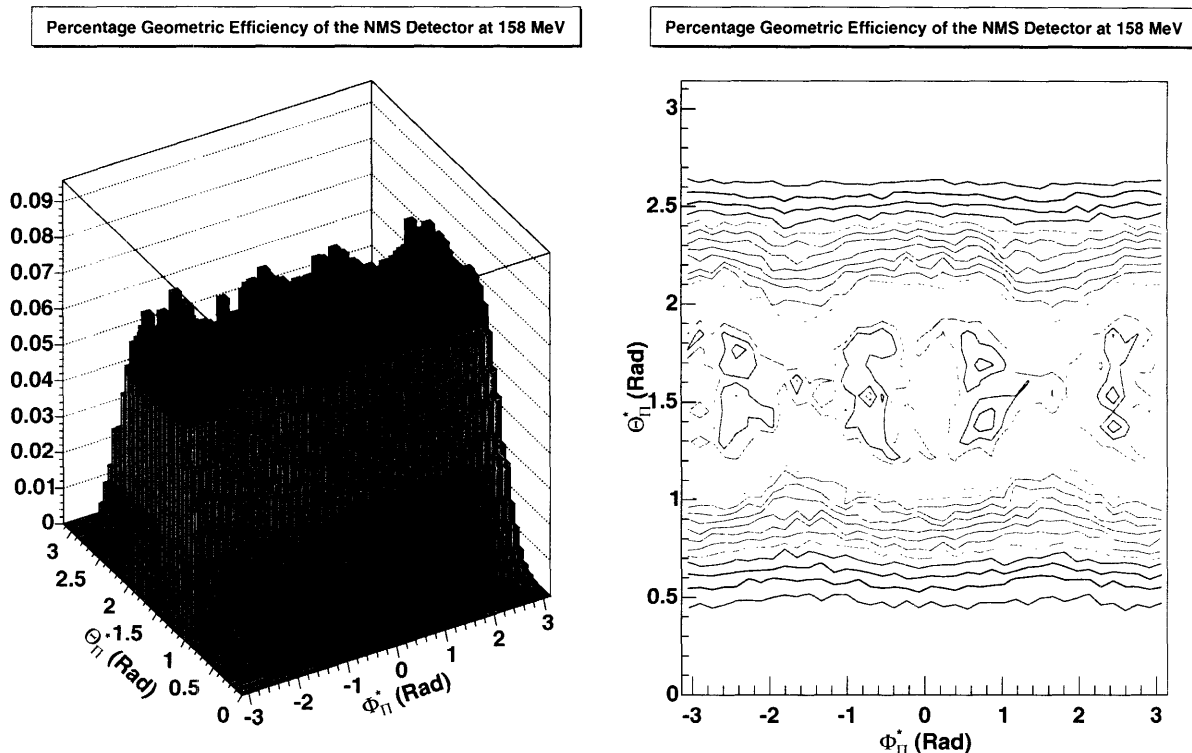


FIG. 6: On the left, the acceptance of the NMS detector for 158 MeV pion production shown as a 2-D histogram. The colors indicate the 0-30%, 30%-70%, and 70%-100% regions of the histogram. On the right, a contour map of the acceptance with 12 equidistant contour levels.

the pion CM angles, these errors are the main contribution to the error in our fits. There is one further important detail about our simulated experimental setup. I have assumed that I can separate the photons registered in the detector produced by π_0 -proton events from all other background. This is a significant assumption (aside from standard noise removal) because some proposed target contain carbon, which exhibits a cross section nearly 100 times larger than the proton in the near threshold region. This difficulty will have to be avoided by one of three methods: 1) Use a pure liquid hydrogen target. 2) Use an active scintillator target so that the amount of recoil from a count can be registered. 3) Remove most of the detected counts from carbon by observed energetic differences. I have assumed a pure liquid hydrogen target for my simulations but any one of these strategies should produce the same results. With this description of the apparatus, I have fit the cross section of pion production in various ways.

3. FIT RESULTS

I used the Minuit utility to perform χ^2 fits on the reconstructed pion CM angles. I started by fitting the coefficients of the cross section as presented in section 1.1 using the exact pion angles assuming a 4π solid angle coverage detector and zero errors to assess the accuracy of the fitting mechanism. The results of this test fit are shown in table I. I have only presented the results for the examples of the coefficients given in that section in the table. The plots on the other hand include all 14 coefficients that I used. I have also presented figures comparing the input cross section and the fit cross section with the detected counts and statistical errors superimposed. I have taken slides of the plots at different

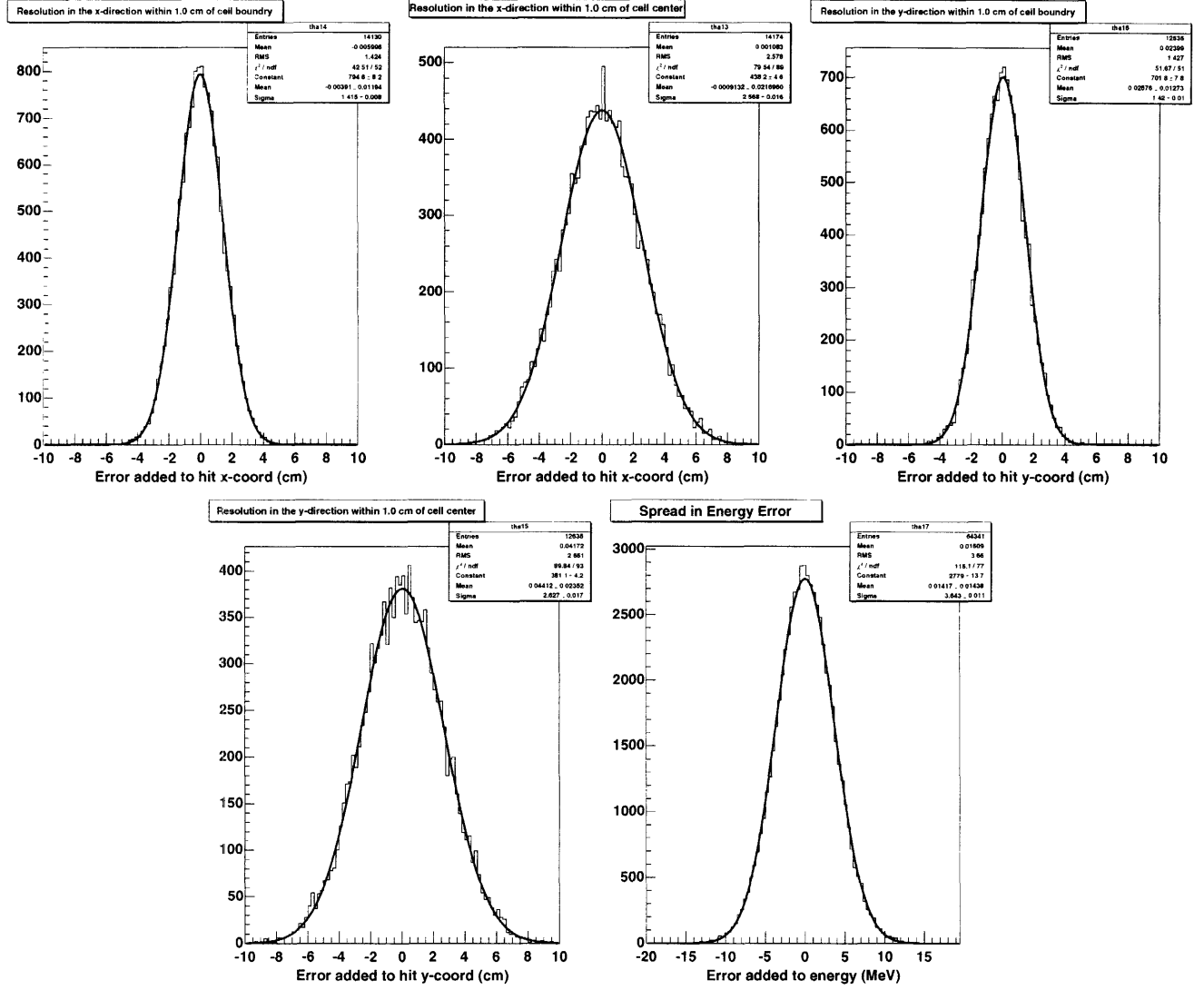


FIG. 7: 1) Error added to x-position on the detector within 1 cm of a crystal boundary. 2) Error added to x-position on the detector within 1 cm of a crystal center. 3) Error added to y-position on the detector within 1 cm of a crystal boundary. 4) Error added to x-position on the detector within 1 cm of a crystal center. 5) Error added to the energy over all events.

values of ϕ_π^* so that comparisons between the fits can be made easily (see figure 10). One further test of the fits is the distribution of bins on either side of the fit. Figure 11 shows that the input and fit have approximately the same number of bins above and below them. The calculation of the bins for these distributions is given by equation 23. When we normalize the histograms (as in the figure), they should match the normal distribution in equation 24.

$$\frac{\text{Count}_{bin} - \text{Counts}_{formula}}{\sqrt{\text{Counts}_{formula}}} \quad (23)$$

$$\frac{1}{2\sqrt{\pi}} e^{-x^2/2} \quad (24)$$

For the true test of the NMS detector, I used the same functions as for the zero error, 4 Π detector and replaced the exact angles with the reconstructed angles from the detector apparatus. In these fits, I could only use the approximately 63,000 (out of the 1.43 million produced) detected events so the statistical errors are much higher. The

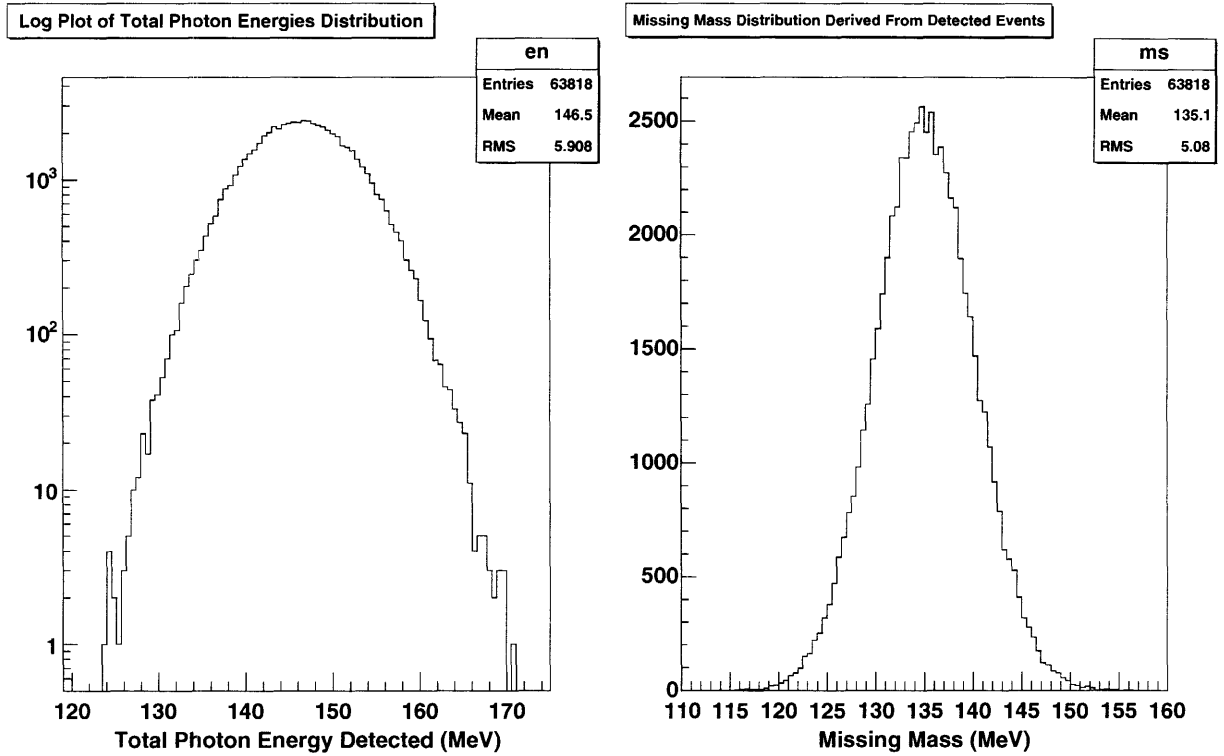


FIG. 8: On the left, a log-linear plot of the addition of the two photon energies as detected. On the right, the missing mass calculation. The correct value should be the mass of the pion 135 MeV and we see that the distribution mean is 135.1.

TABLE I: Table of fit coefficients with zero error, full coverage detector. This comparison shows how closely we can expect the fitter to come to the input cross section with only statistical limitations. The shown coefficients correspond to those shown in equations 6-9. For this fit, $\chi^2/(\text{degrees of freedom}) = 2374.73/1586$. This value is a bit high because the fit is closer to correct than it should be at these statistics.

Coefficient	Input (μ barns)	Output (μ barns)	Std. Dev. (μ barns)	Input-Output (# of Std. Devs.)	Error/Input
aT	0.135769	0.135603	0.000622796	0.266929	0.00458717
bT	-0.0166644	-0.0166532	0.000676915	0.0165705	0.0406204
cT	-0.0374773	-0.0376701	0.00130208	0.148066	0.034743
aTn	0.0605117	0.0601603	0.00832752	0.0422005	0.137618
bTn	-0.00208738	-0.00217272	0.0187665	0.00454696	8.99046
aTT	-0.0113103	-0.0113815	0.000836602	0.0851296	0.0739681
aTTn	-0.00269293	-0.00299265	0.00928934	0.0322642	3.44953
bTTn	0.000221836	0.000116612	0.0209251	0.00502861	94.327

reconstructed cross section that has been scaled by the acceptance can be seen in figure 14. In addition of course, all the detector inaccuracies contribute. Some example coefficient data is shown in table II. Phi slices of this fit are shown in figure 12 and the distribution of bins around the fit is shown in figure 13. The data shows that the coefficients are mostly within one standard deviation and the χ^2 per degree of freedom is close to 1. Thus I believe that this fit is correct and represents how well we could determine these coefficients with this method given the apparatus.

I have also carried out the alternative method of splitting up the cross section detailed in section 1.1. I ran each of the four possible helicities for 50 hours so that the total statistics on this method was actually twice that of the previous fit. The coefficient fits from this method were comparable to the above method and the phi slices for the

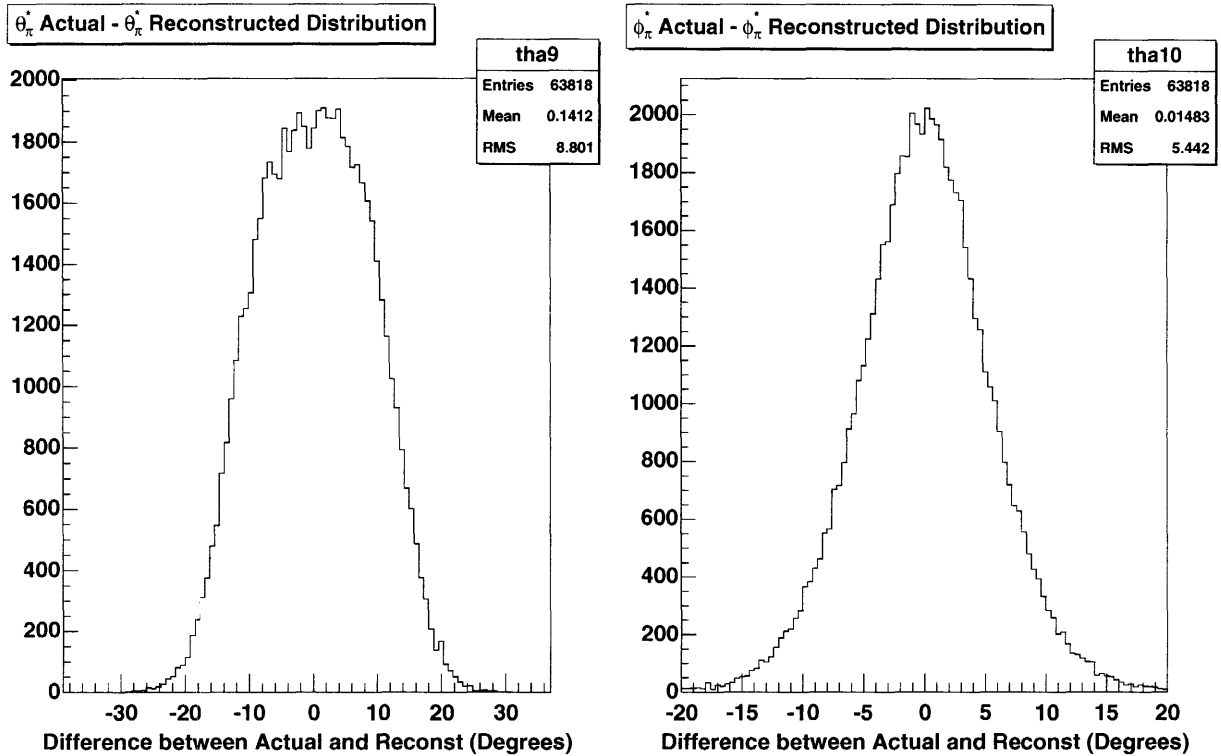


FIG. 9: The distributions of errors in θ_π^* and ϕ_π^* reconstruction over all simulated events on the left and right, respectively.

TABLE II: Table of fit coefficients with full simulated NMS detector. The shown coefficients correspond to those shown in equations 6-9. For this fit, $\chi^2/(\text{degrees of freedom}) = 679.815/666$. This value close to 1 shows that the fit is good and the errors are representative.

Coefficient	Input (μ barns)	Output (μ barns)	Std. Dev. (μ barns)	Input-Output (# of Std. Devs.)	Error/Input
aT	0.135769	0.130915	0.00314928	1.54129	0.0231959
bT	-0.0166644	-0.0167	0.00709602	0.00502227	0.425819
cT	-0.0374773	-0.0370705	0.0199343	0.0204075	0.531903
aTn	0.0605117	0.0594207	0.00281366	0.387745	0.0464978
bTn	-0.00208738	-0.00284163	0.00840203	0.0897696	4.02515
aTT	-0.0113103	-0.00939365	0.00352809	0.543254	0.311936
aTTn	-0.00269293	-0.00362589	0.0049594	0.188119	1.84164
bTTn	0.000221836	-0.00053946	0.0148996	0.0510951	67.1649

different portions of the cross section are shown in figures 15-18. The important comparison between the two methods is the ratio of coefficient magnitude to error magnitude. If the error on a coefficient is nearly the same as the value of that coefficient, then the fit is nearly meaningless. The smaller coefficients will contribute less to the cross section and thus will be harder to fit and have larger errors. In figure 19, I have plotted these error ratios on a log-log scale for the single complete cross section fit and the breaking up of the cross section into pieces. The split fit actually has higher errors on the small coefficients and on one of the large coefficients than the single fit even with double the running time. The split fit does improve the error on many of the larger multipoles though it is not clear whether this could be due to increased statistics. Determining which method to use for the actual experiment should be approached as a trade-off between the accuracies of different multipoles.

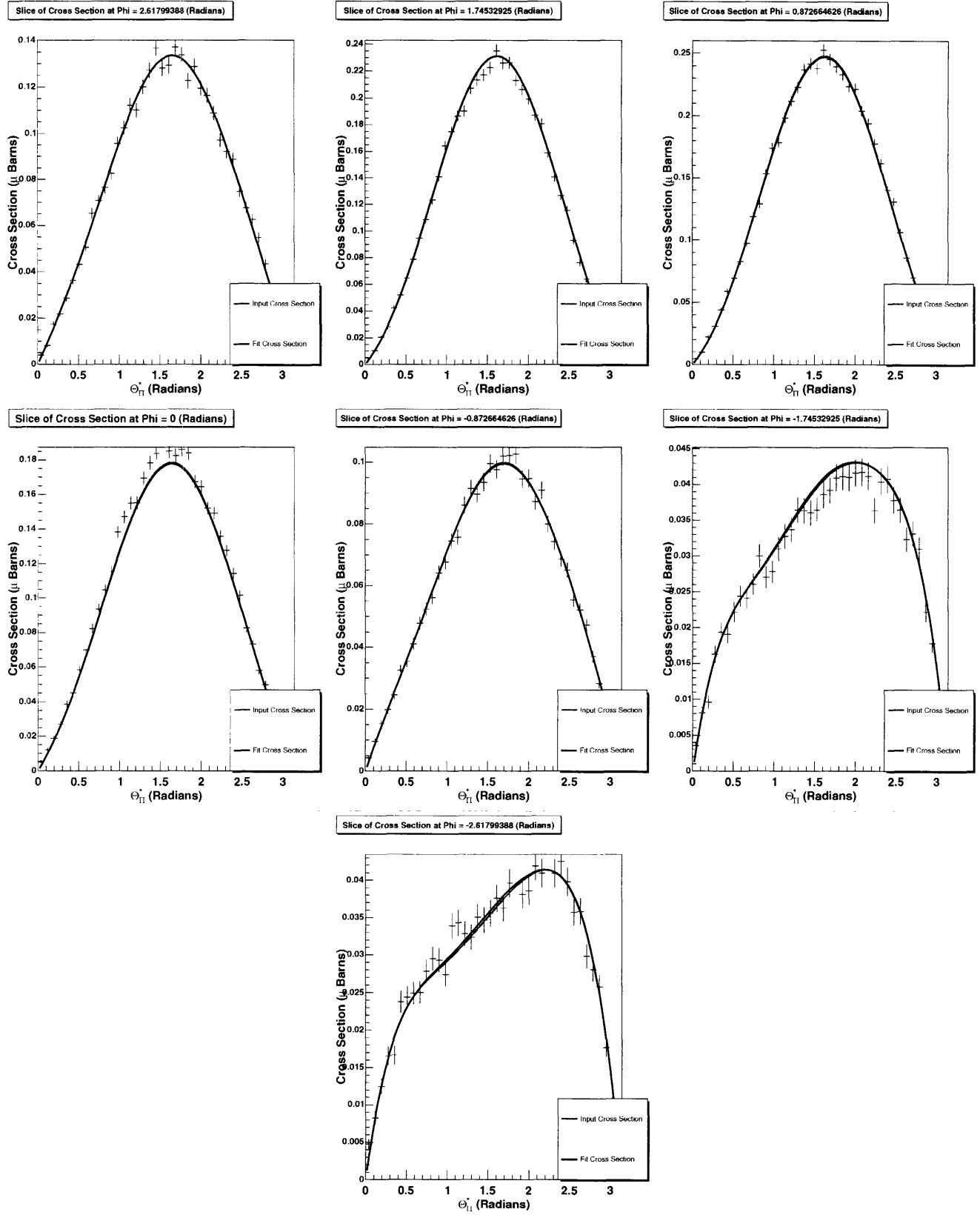


FIG. 10: Slices of the full 14 coefficient fit with perfect accuracy and a 4π (full coverage) detector at phi angles 150, 100, 50, 0, -50, -100, -150 degrees, respectively. These demonstrate that the input and fit functions are nearly the same. The red curve shows the input function used to generate the data and the blue curve shows the fit.

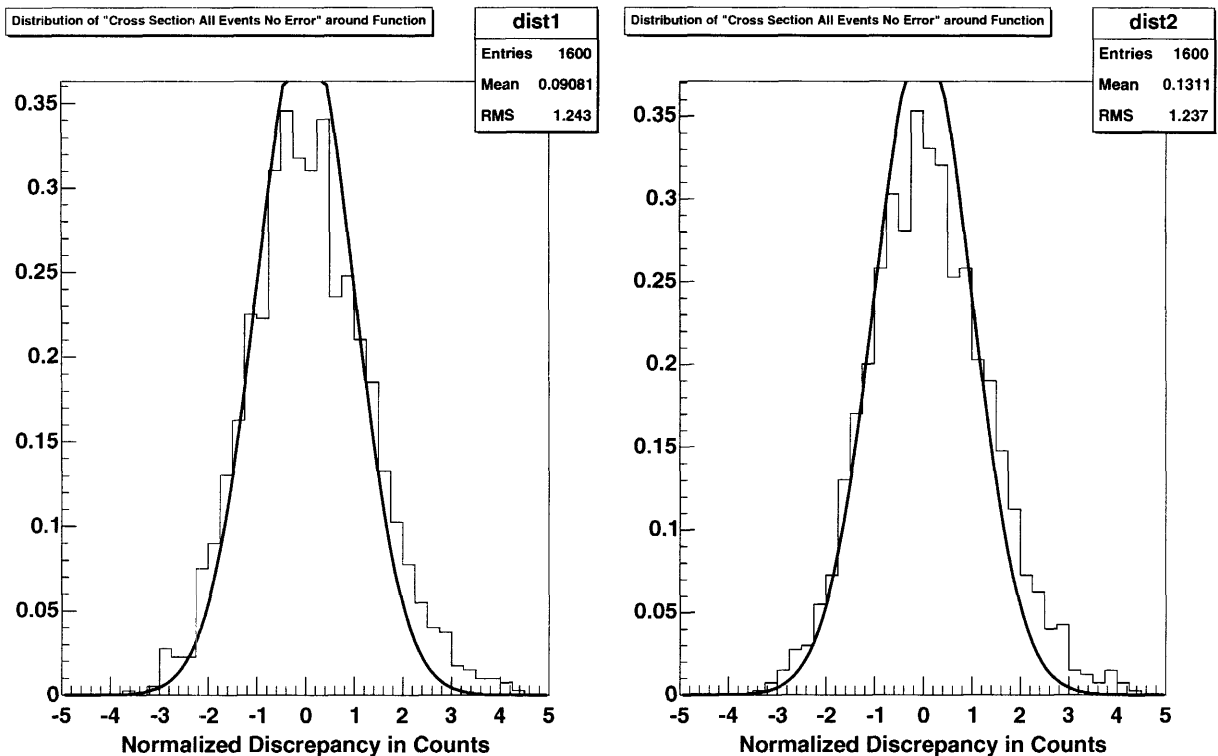


FIG. 11: Normalized distribution of bins around the input and perfect fit functions on the left and right, respectively.

4. CONCLUSIONS AND FUTURE WORK

I detailed the theory motivating this near threshold polarized pion photoproduction experiment. I simulated the NMS detector that has been proposed for this experiment. I was able to examine the cross section coefficient fit accuracy and ensure the goodness of my fits. I compared different methods of using the polarization of target and detector to separate parts of the cross section. I found a trade off between the accuracies of larger and smaller coefficients such that splitting the cross section gave less accurate results for small coefficients. If better accuracy than that presented is desired, then we may want to look for a detector with larger coverage and better position resolutions.

We are planning a number of improvements in the future. Although I was able to fit the coefficients of the cross section, fitting the multipoles proved challenging and still does not function correctly. The non-linearity and correlation of observables that occurs when using multipole definitions makes χ^2 fitting difficult even when giving the correct initial values. While we can verify that these values give a value for χ^2 per degree of freedom near 1, the fitter continues looking for a minimum until it quits without convergence. Thus the errors on these multipole fits have yet to be determined. The coefficient and multipole expansions presented in section 1.1 ignore all but the S and P wave contributions. We believe that there are significant contributions to the cross section from higher partial waves.

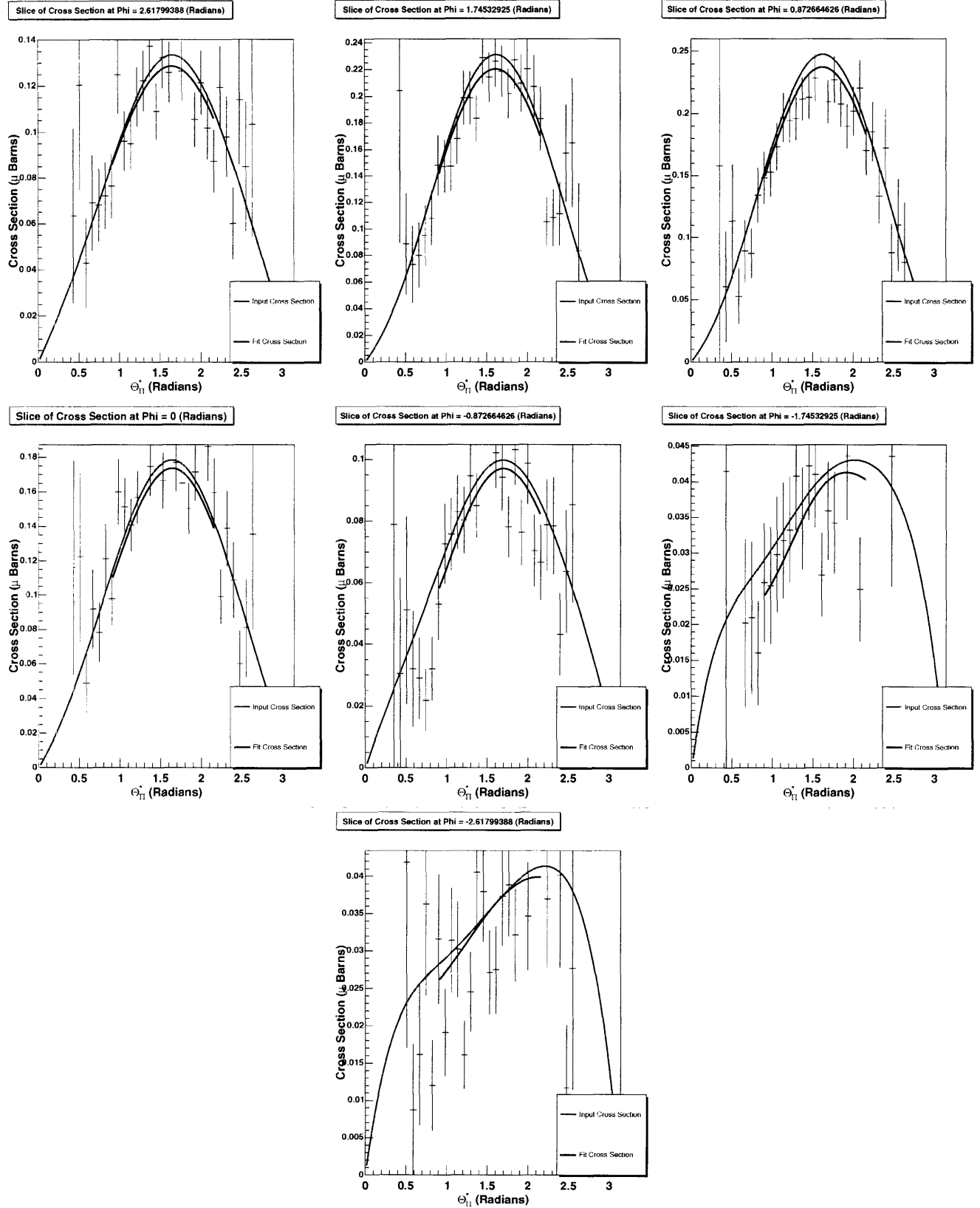


FIG. 12: Slices of the full 14 coefficient fit with NMS detector and all expected errors at ϕ angles 150, 100, 50, 0, -50, -100, -150 degrees, respectively. We see that while there are significant discrepancies between the functions and the bins, both functions are within the errors on each data point. The red curve shows the input cross section used to generate the data and the blue curve shows the fit. The fit curve is only defined on the region of the cross section where the acceptance is high enough as defined in section 2.1. Thus the blue curve is only shown on that region.

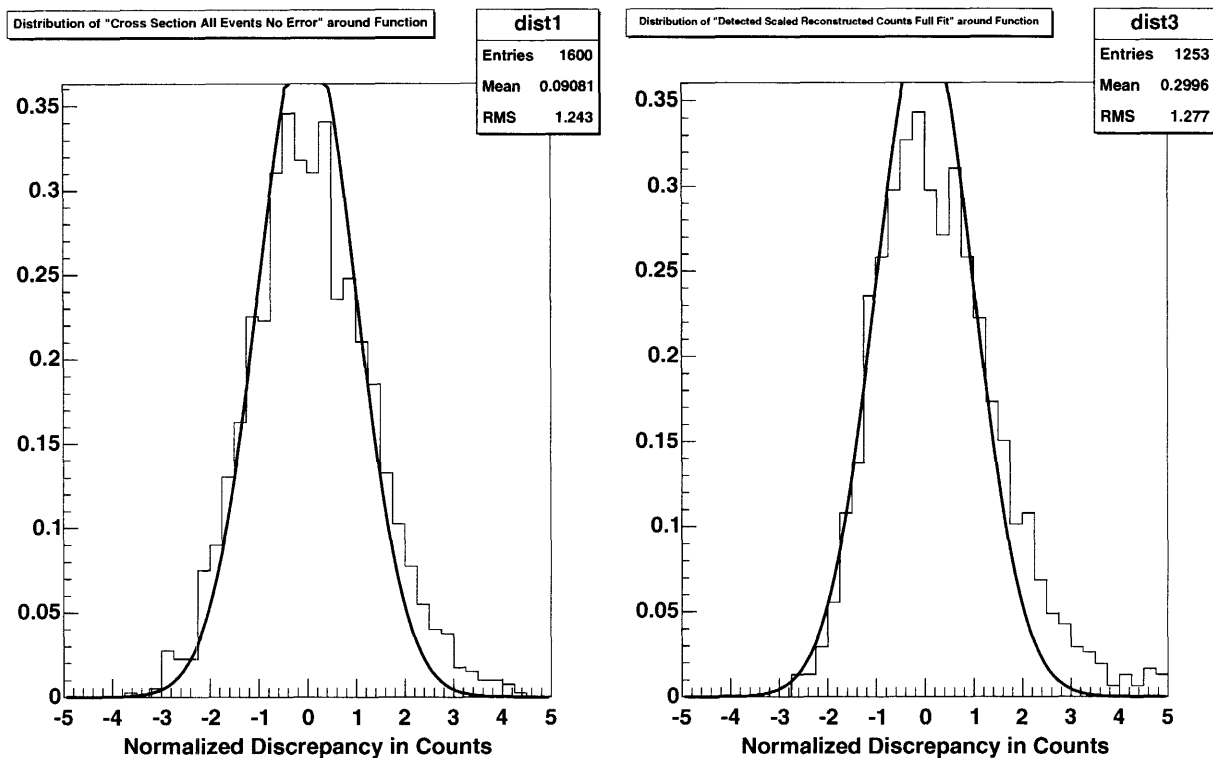


FIG. 13: Normalized distribution of bins around the input and simulated NMS fit functions on the left and right, respectively.

There are methods for computing these contributions and we will be incorporating them into the simulation.

-
- [1] A. Schmidt et al., Phys. Rev. Lett. 87, 232501(2001).
 - [2] S. Weinberg, Transactions of the N.Y.Academy of Science Series II 38, 185 (1977).
 - [3] D. Drechsel and L. Tiator, J. Phys. G: Nucl. Part. Phys. 18,449(1992). A.S. Raskin and T.W. Donnelly, Annals of Phys.(N.Y.)191, 78(1989).
 - [4] *Photo- and Electroproduction of Eta Mesons* G. Knichlein, D. Drechsel, L. Tiator, Z. Phys. A 352 (1995) 327
 - [5] A.M. Bernstein, et al., Photopion Production Measurements: Tests of QCD Chiral Dynamics, Internal Proposal Draft (Feb. 9, 2005)
 - [6] D. Drechsel *et al.*, Nucl. Phys. **A645**, 145 (1999). <http://www.kph.uni-mainz.de/MAID/>
 - [7] S.S. Kamalov, Guan-Y. Chen, Shin-Nan Yang, D. Drechsel, L. Tiator, Phys.Lett.B522:27-36,2001. S.N. Yang, Guan-Yeu Chen, S.S. Kamalov, D. Drechsel, L. Tiator, Nucl. Phys. A 737:248-252 (2004). <http://www.kph.uni-mainz.de/MAID/dmt/dmt2001.html>
 - [8] M. Ahmed, Personal communication on the properties of the NMS detector (Feb. 2005).

5. ACKNOWLEDGEMENTS

I would like to thank Professor Aron Bernstein for patient help and insightful counsel. Professor Bernstein gave me this important opportunity and he remained confident in me even when work progressed more slowly than we had

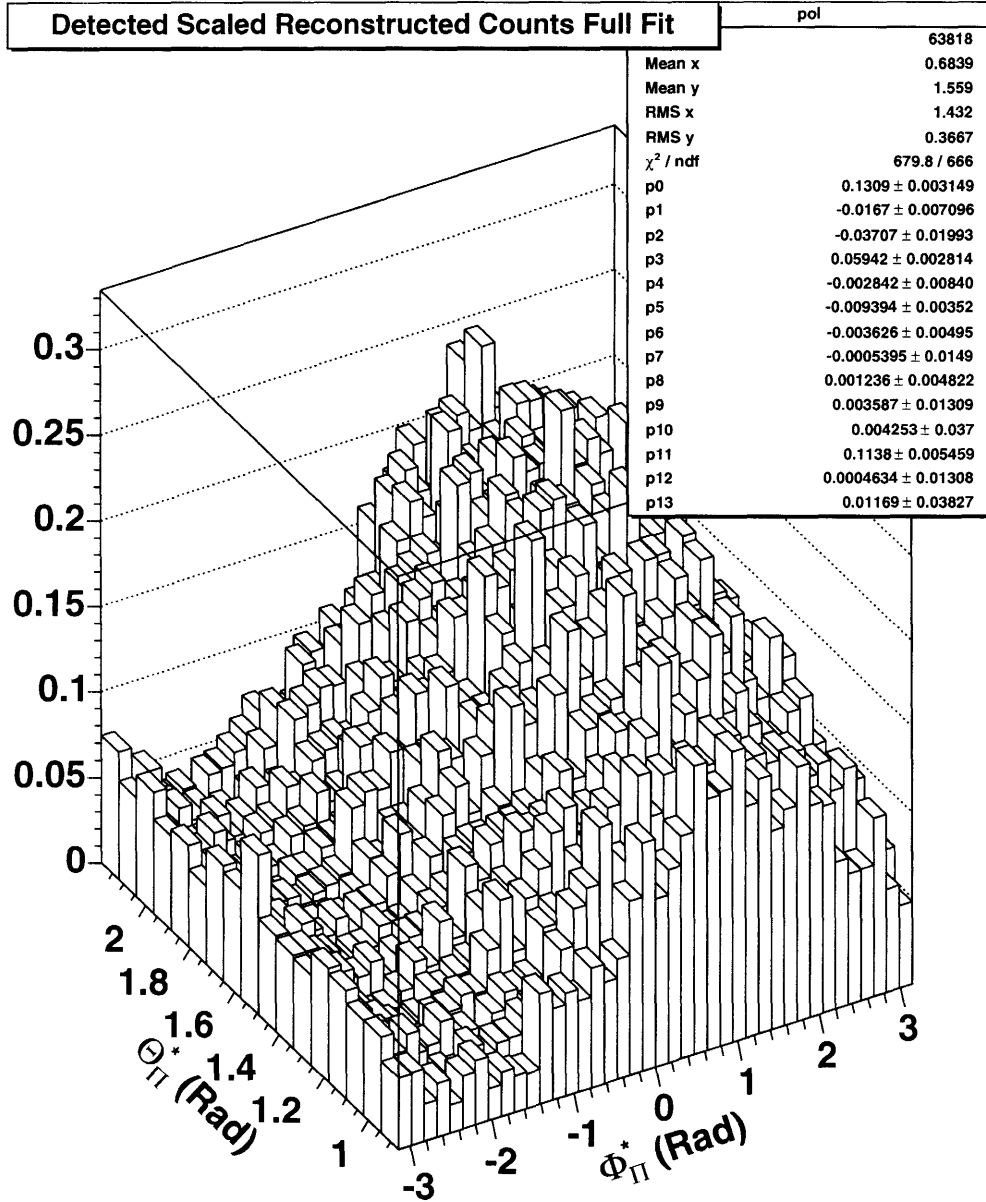


FIG. 14: The reconstructed cross section scaled by the acceptance and limited to the reliable (> 30%) region

hoped. I have been fortunate to learn from him and work with him for the past year and most of the credit for this thesis is due to him. I would also like to thank Dr. Doug Hassell for contributing the code, on which I based my program and for providing assistance along the way. Paul Kingsberry was an excellent companion in this work and gave me insight into how my problems could be solved. Sean Stave was always willing to track down even the most elusive bug with me and he shared his expert knowledge of ROOT whenever I had a question. I am grateful to have work with all these people and I hope to possibly work with them again in the future.

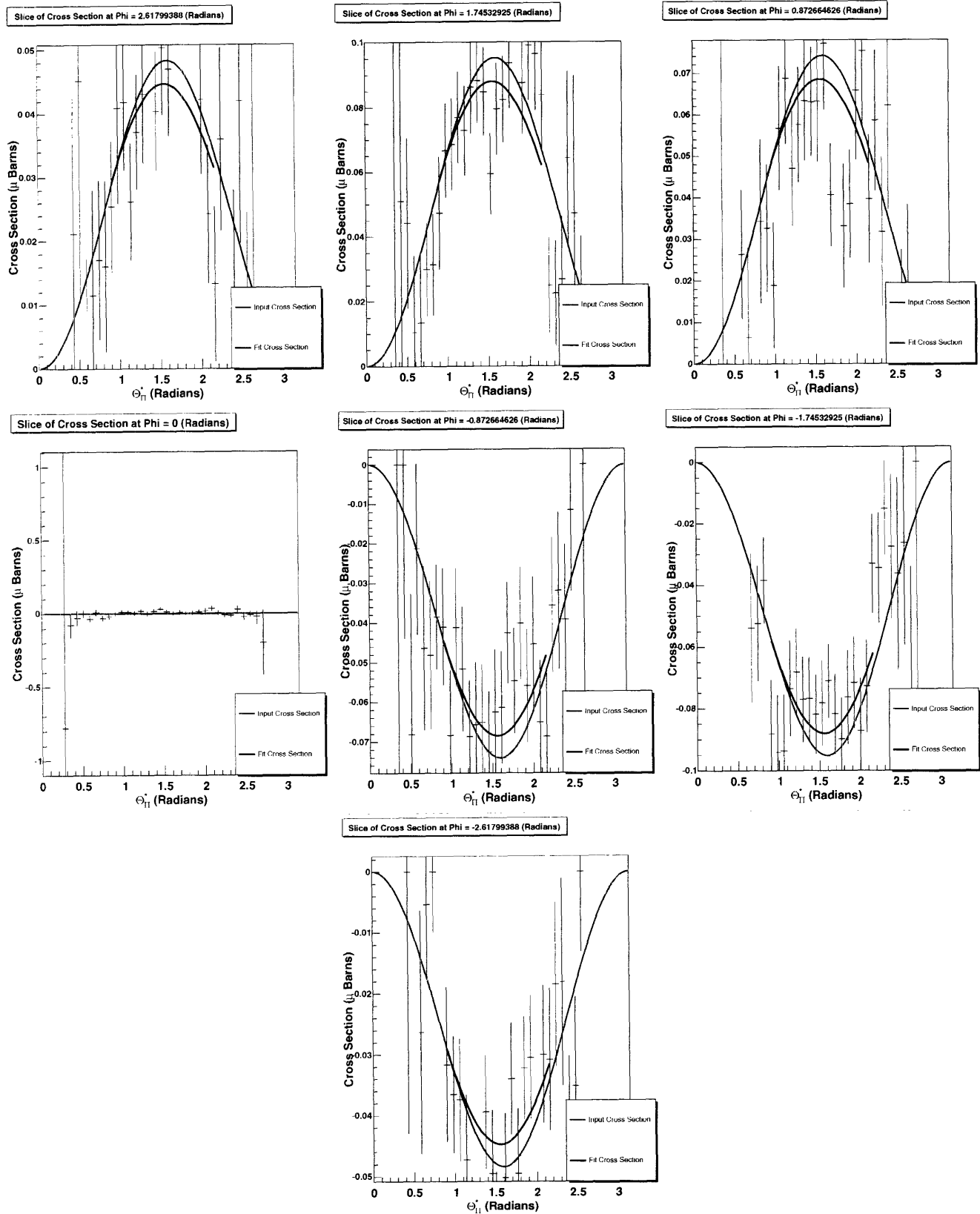


FIG. 15: The fit slices of the portion of the cross section defined by equation 11 using the NMS detector and all expected errors at ϕ angles 150, 100, 50, 0, -50, -100, -150 degrees, respectively. The red curve shows the input cross section used to generate the data and the blue curve shows the fit. The fit curve is only defined on the region of the cross section where the acceptance is high enough as defined in section 2.1. Thus the blue curve is only shown on that region.

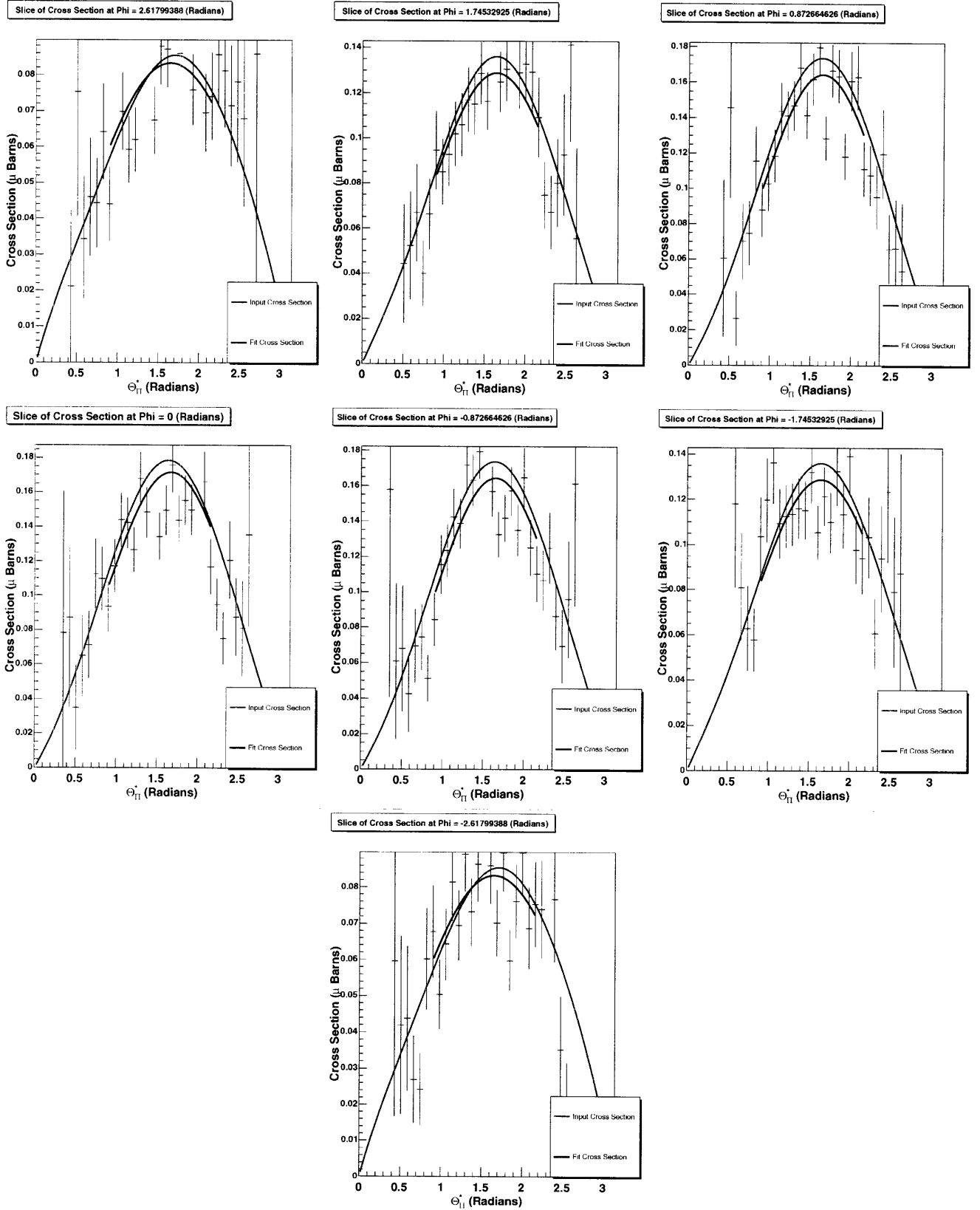


FIG. 16: The fit slices of the portion of the cross section defined by equation 12 using the NMS detector and all expected errors at phi angles 150, 100, 50, 0, -50, -100, -150 degrees, respectively. The red curve shows the input cross section used to generate the data and the blue curve shows the fit. The fit curve is only defined on the region of the cross section where the acceptance is high enough as defined in section 2.1. Thus the blue curve is only shown on that region.

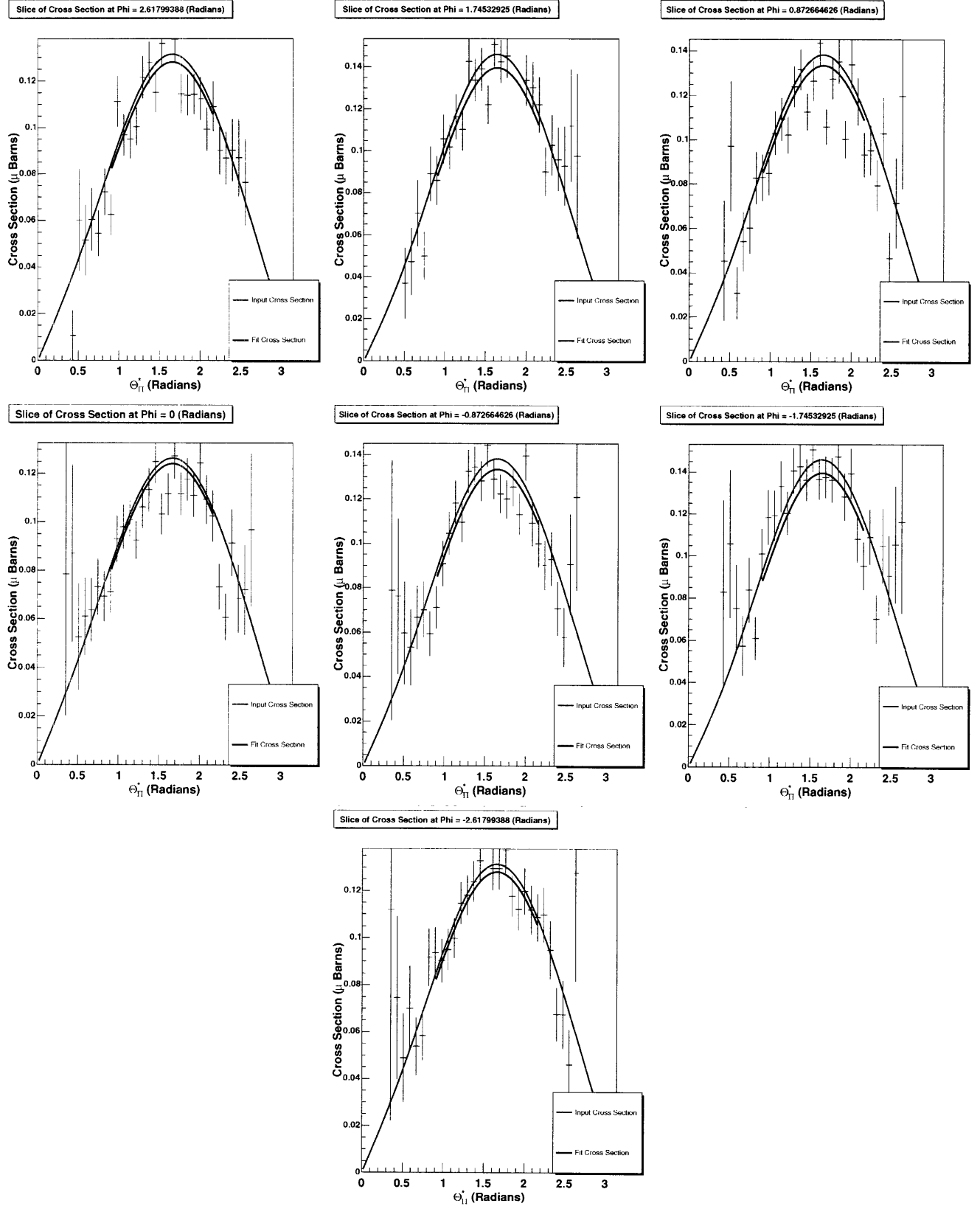


FIG. 17: The fit slices of the portion of the cross section defined by equation 13 using the NMS detector and all expected errors at ϕ angles 150, 100, 50, 0, -50, -100, -150 degrees, respectively. The red curve shows the input cross section used to generate the data and the blue curve shows the fit. The fit curve is only defined on the region of the cross section where the acceptance is high enough as defined in section 2.1. Thus the blue curve is only shown on that region.

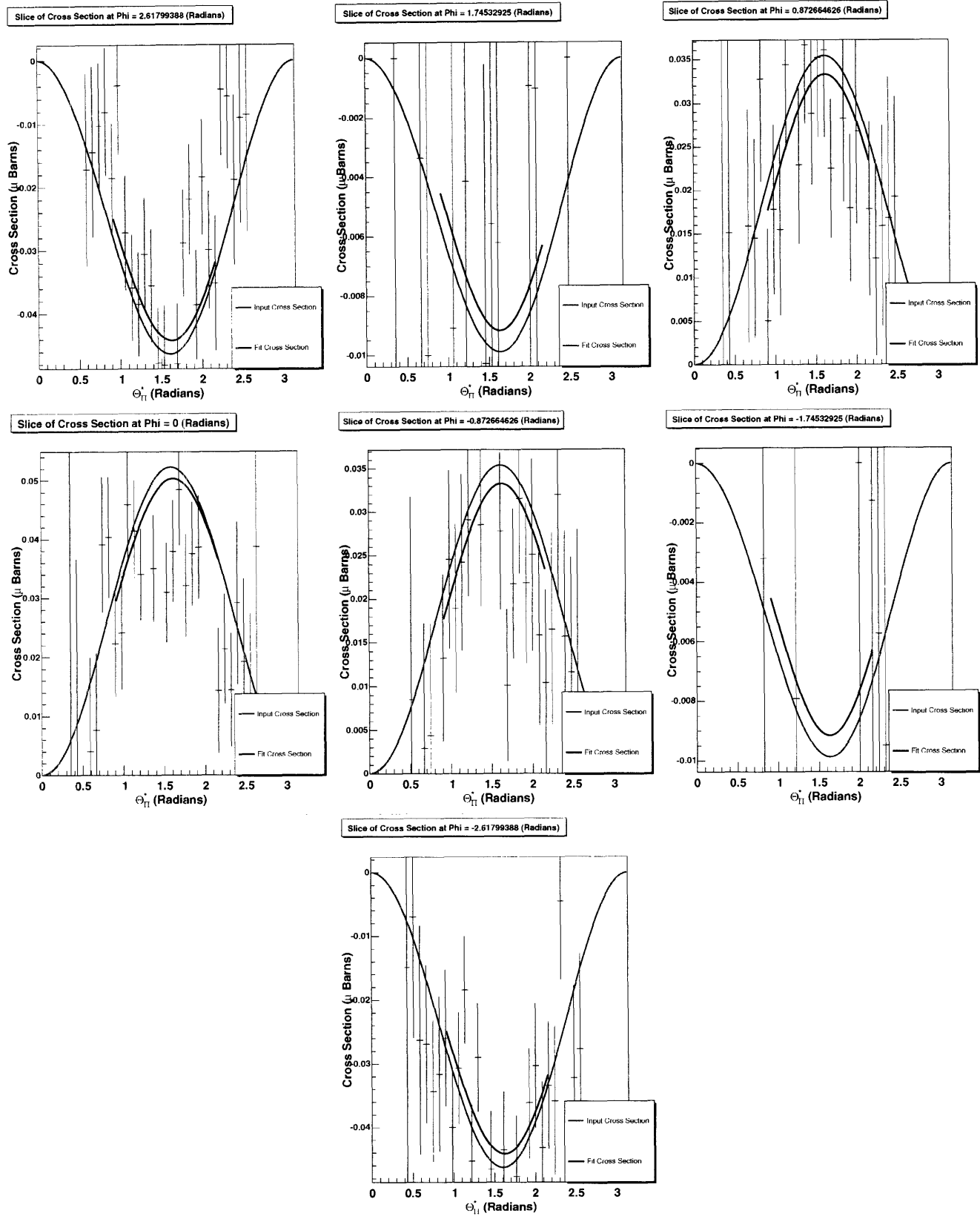


FIG. 18: The fit slices of the portion of the cross section defined by equation 14 using the NMS detector and all expected errors at ϕ angles 150, 100, 50, 0, -50, -100, -150 degrees, respectively. The red curve shows the input cross section used to generate the data and the blue curve shows the fit. The fit curve is only defined on the region of the cross section where the acceptance is high enough as defined in section 2.1. Thus the blue curve is only shown on that region.

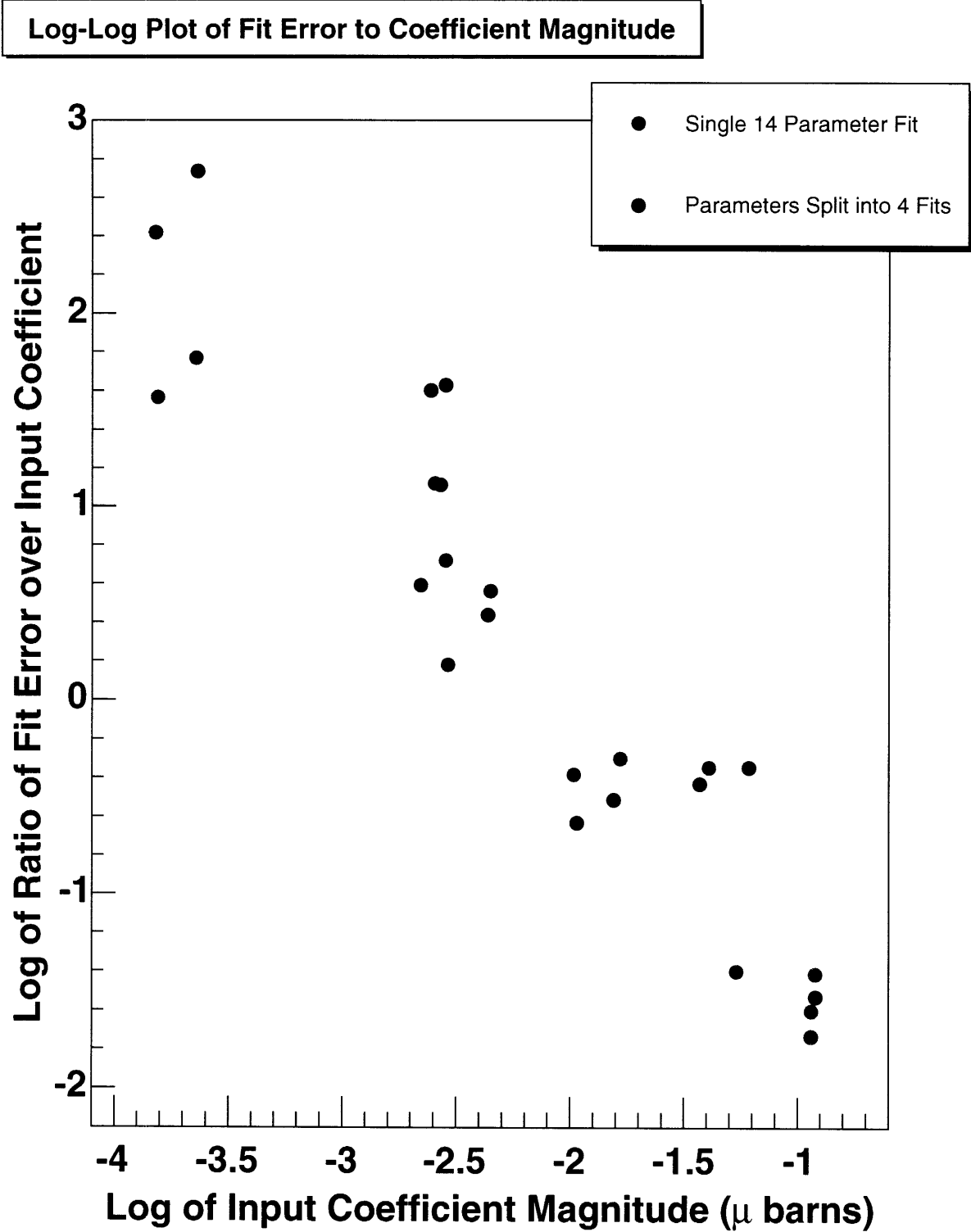


FIG. 19: Log-log plot of the ratio of the error in the fit to the magnitude of the coefficient as a function of the magnitude of the coefficient. We see that as the coefficient gets smaller the less accurate our fits are for it as we would expect.

APPENDIX A: SIMULATION SCRIPT NAMES AND FUNCTIONS

1. pi0_photo_sp3.C is the current data generation script for use with a single target and beam polarization (use with pi0hctmsp8.C below)
2. pi0_photo_mp.C is the data generation script for multiple target and beam helicities. It must be run once for each polarization setting but it is more convenient to use than any other script. (use with pi0hctmp.C below)
3. pi0_photo_sp2.C is the current data generation script for computing detector acceptance. It can be set to multiple types of simple cross sections but its default is a flat cross section. (The exact cross section does not really matter for acceptance.)
4. pi0hctmsp8.C is the current data analysis script for a single target polarization. It includes fits for both coefficients and multipoles and a number of error checking figures. If performing extensions on the simulation, this is the script, from which it should be built.
5. pi0hctmp.C is the data analysis script for analyzing all four types of detector polarization together so that it can extract different pieces of the cross section. Contains most of the same functions as pi0hctmsp8.C but most have been commented out.
6. pi0hcsfull.C is the specialized data analysis script for reading in the data meant for acceptance calculation and saving the acceptance to the root file geomeff2dfull.root for all other analysis scripts to use.

To execute the currently configured simulation from scratch (to configure a simulation such as changing the run time, you must understand the internals of the scripts), perform the following actions:

1. Start root
2. Load pi0_photo_sp2.C (the command is `.L pi0_photo_sp2.C`)
3. Run `main()` (will take a while to execute)
4. Exit root (recommended but not required)
5. Start root
6. Load pi0hcsfull.C (now the acceptance has been created)
7. Run `pi0_hits()`
8. Exit root
9. Start root
10. Load pi0_photo_sp3.C (should not take too long)
11. Run `main()`
12. Exit root

13. Start root
14. Load pi0hctmisp8.C
15. Run pi0_hits()
16. Examine simulation results
17. Exit root